REVISION 1

Reduced charge transfer in mixed-spin ferropericlase inferred from its high-pressure refractive index

Lukas Schifferle[1,2], Sergio Speziale[1], Björn Winkler[3], Victor Milman[4], Sergey S. Lobanov[1,2*]

[1]GFZ German Research Center for Geosciences, Telegrafenberg, 14473 Potsdam, Germany

[2]Institute of Geosciences, University of Potsdam, Karl-Liebknecht-Straße 24-25, 14476 Potsdam, Germany

[3]Institute for Geosciences, Goethe-University Frankfurt, Altenhöferallee 1, 60438 Frankfurt am Main, Germany

[4]Dassault Systèmes BIOVIA, 22 Science Park, Cambridge CB4 0FJ, United Kingdom

*Email: slobanov@gfz-potsdam.de

ABSTRACT

Physical properties of mantle minerals are essential for comprehensive geodynamic modelling. High-pressure experiments allow measurements of physical properties but fundamental insights into their evolution with pressure are often experimentally inaccessible. Here we report the first *in situ* experimental determination of the optical refractive index, its wavelength-dispersion, and optical absorption coefficient of ferropericlase up to ~140 GPa at room temperature. All these properties change gradually in dominantly high-spin (below ~50 GPa) and low-spin (above ~80 GPa) ferropericlase. However, in the mixed-spin state (*i.e.,* significant presence of both high- and low-spin iron), the index dispersion and the absorption coefficient decrease by a factor of three and ~30 %, respectively. These anomalies suggest that charge transport by small polaron is reduced in mixed-spin ferropericlase, providing fundamental insights into the factor-of-three lower electrical conductivity of ferropericlase at ~50-70 GPa.

KEYWORDS

High-pressure, diamond anvil cell, refractive index, ferropericlase, MgO, DFT, spin transition, band gap, electrical conductivity.

1. INTRODUCTION

Physical properties of the Earth's mantle and core are at the center of our understanding of planetary evolution. For example, if the electrical conductivity of the lowermost mantle is sufficiently high, the conducting core and the mantle may exchange angular momentum producing detectable intradecadal signals in the length of day (Duan and Huang, 2020; Holme and de Viron, 2013) or imposing preferred paths of geomagnetic reversals along the Americas or Eastern Asia (Buffett, 2015; Runcorn, 1992). Furthermore, the mantle acts as a filter on the magnetic field of the core; thus, knowledge of the electrical conductivity of the mantle is needed to decipher the dynamo history from the geomagnetic record (Alexandrescu et al., 1999; Bloxham and Jackson, 1992; Constable, 2015). Ferropericlase (Fp), being the second most abundant mineral in the lower mantle and the dominant host of iron (Irifune et al., 2010; Piet et al., 2016), likely governs the bulk electrical conductivity of that region. Accordingly, the electrical conductivity of Fp has been the subject of many experimental and theoretical investigations.

Earlier experimental measurements of electrical conductivity at pressures below ~30 GPa have established that the conductivity of Fp is very sensitive to its overall iron content (Dobson et al., 1997; Hansen and Cutler, 1966; Li and Jeanloz, 1990). Perhaps even more importantly, pressure (*P*), temperature (*T*), and oxygen fugacity, all of which vary in the mantle with depth, affect the conductivity of Fp (Dobson and Brodholt, 2000; Wood and Nell, 1991). Two different charge transfer mechanisms have been identified in Fp. At $T < \sim 1000$ K, the activation energies and the dependence of electrical conductivity on the Fe^{3+}/Fe_{total} ratio indicate that the dominant conduction mechanism is the electron hopping between Fe^{2+} and Fe^{3+} (small polaron) (Dobson et al., 1997; Iyengar and Alcock, 1970). At mantle temperatures ($T > \sim 1000$ K), however, the extant experimental data are consistent with the mechanism that involves Fe-O charge transfer (large polaron) (Dobson et al., 1997). Subsequent measurements to ~100 GPa found that the room-temperature conductivity of Fp increases by a factor of ~10 upon compression to 50 GPa, drops by a factor ~3 at 50-70 GPa, and then either increases upon further compression (Lin et al., 2007) or is almost insensitive to pressure (Ohta et al., 2007). The factor-of-three drop in room-temperature electrical conductivity at 50-70 GPa is concomitant with the iron high-to-low spin transition in Fp (Glazyrin et al., 2016; Lin et al., 2007) and has been attributed to the decreased mobility and/or density of charge carriers (small polaron) in low-spin Fp (Lin et al., 2007; Ohta et al., 2007). Optical studies indirectly support this conclusion as the overall absorbance in the visible range, which is a measure of high-frequency electronic conductivity, decreases with pressure in low-spin Fp (Goncharov et al., 2006; Keppler et al., 2007; Schifferle and Lobanov, 2022). This decrease in absorbance, however, is somewhat questionable because of the unknown sample thickness at high pressure, which is also expected to decrease with pressure in a strongly non-isotropic fashion (Lobanov and Geballe, 2022). Reliable *in situ* measurements of sample thickness are thus needed to quantify the absorption coefficient of Fp at high pressure and to resolve whether the electrical conductivity of Fp is linked to its optical properties.

DOI: https://doi.org/10.2138/am-2023-9100. http://www.minsocam.org/

The thickness of (semi)transparent samples in diamond anvil cell (DAC) experiments can be accurately measured if the refractive index of the sample is known. The refractive index and its wavelength-dispersion also provide information on the electronic structure of materials. Pressure-induced changes in the electronic conductivity (*e.g.* due to small polarons) may thus be accompanied by changes in the refractive index. To the best of our knowledge, the refractive index of ferropericlase at elevated pressures has never been characterized. Recently, we developed a method to measure the refractive index and its wavelength-dependence of fully transparent solids compressed in a DAC to pressures greater than 100 GPa (Lobanov et al., 2022; Schifferle et al., 2022). In the present work, we build up on that method to make it applicable for semitransparent samples and report the refractive index of high spin (HS), mixed spin (MS), and low spin (LS) ferropericlase. Our results show that the refractive index of Fp in the visible spectral range is largely independent of pressure or iron spin state. The wavelength-dispersion of the refractive index is also nearly invariant in the HS and LS Fp but is reduced abruptly by a factor of three in the MS state. The absorption coefficient also decreases by ~35% at the onset of the spin transition. Our observations allow an alternative interpretation of the previous high-pressure electrical conductivity data. We suggest that the mobility and/or density of small polarons is reduced only in the MS regime, unlike previous studies that proposed reduced small polaron transport in LS Fp.

2. EXPERIMENTAL METHODS

Samples and diamond anvil cell loading

All high-pressure experiments were performed using symmetrical DACs equipped with diamond pairs featuring beveled 300/100 μm or flat 300 μm culets. The beveled diamonds feature 300 μm culets at 8° to a single 100 μm central flat. Rhenium gaskets indented to a thickness of 15-20 μm were laser-drilled to create cylindrical holes with diameters of ~45 μm (when 300/100 μm culets were used) or ~140 μm (when 300 μm culets were used), which served as sample chambers. For each loading we selected fragments of the samples with appropriate dimensions to fill the DAC sample chamber, placed the samples without any pressure-transmitting medium, immediately sealed the DAC assembly and increased the pressure to ~20-30 GPa producing optically homogenous samples, which is required for refractive index measurements described below. We used synthetic single-crystalline samples of ferropericlase of two different compositions: $(Mg_{0.87}Fe_{0.13})O$ and $(Mg_{0.76}Fe_{0.24})O$, further referred to as Fp13 and Fp24 to indicate their iron content. Fp13 was produced by Fe diffusion into an MgO crystal in a gas-mixing furnace at ambient pressure (Lobanov and Speziale, 2019). Fp24 was synthesized by Caterina Melai (Aprilis et al., 2020) in a 10/5 multi-anvil assembly at 15 GPa and 1800 °C using starting material from (Longo et al., 2011). Electron energy loss spectroscopy yielded an $Fe^{3+}/\sum Fe_{total}$ ratio of ~0.1 for Fp13 (Lobanov and Speziale, 2019), however, its Fe^{3+} content might be considerably lower as discussed in (Schifferle and Lobanov, 2022). The $Fe^{3+}/\sum Fe_{total}$

ratio of Fp24 is ~0.02, based on Mössbauer spectroscopy measurements (Aprilis et al., 2020). Because the fragments of Fp13 and Fp24 were effectively crushed in the DAC sample chamber upon sealing and pressure increase, they are likely present in the form of coarse powder at high pressure (although this has not been verified by x-ray diffraction). The pressure at the center of the sample chamber was gauged following the diamond Raman edge method with a relative uncertainty of ~5% (Akahama and Kawamura, 2006).

Refractive index measurements

Because of significant light attenuation in Fp13 and Fp24 over thicknesses characteristic of samples in DAC, we needed to extend the reflectivity method used previously to study transparent samples (Lobanov et al., 2022; Schifferle et al., 2022; van Straaten and Silvera, 1988; Zha et al., 2007) to semi-transparent (absorbing) samples. The approach is based on the Fresnel equation for normal incidence, where the measured reflectivity of the diamond-sample interface ($R_{dia\text{-}smp}$) is related to the refractive index n of the sample (n_{smp}) and diamond (n_{dia}), and the imaginary part of the refractive index of the sample (κ_{smp}):

$$R_{dia-smp} = \frac{(n_{smp}-n_{dia})^2+\kappa_{smp}{}^2}{(n_{smp}+n_{dia})^2+\kappa_{smp}{}^2} \quad \text{(Eq. 1)}$$

Previous reports on the absorption coefficient of ferropericlase indicate that for Fp13 and Fp24 κ_{smp} is small (~0.01 for the studied pressure range, see Supplementary Data for further details) and can thus be considered zero. Nonetheless, quantifying light attenuation in ferropericlase due to absorption is necessary for the determination of $R_{dia\text{-}smp}$:

$$\frac{I_1+I_2}{I_0} = R_{dia-smp} + T^2(R_{dia-smp}{}^3 - 2R_{dia-smp}{}^2 + R_{dia-smp}) \quad \text{(Eq. 2)},$$

where I_0, I_1, and I_2 are individual reflections defined graphically in **Figure 1 A**. T is sample transmission ($T = 0$ for opaque and $T = 1$ for transparent samples). We independently express T through I_T/I_{noDAC}:

$$\frac{I_T}{I_{noDAC}} = T(R_{dia-smp}{}^2 - 2R_{dia-smp} + 1)(1 - R_{dia-air})^2 \quad \text{(Eq. 3)}$$

where I_T and I_{noDAC} are the signals measured through the sample and without the DAC and $R_{dia\text{-}air}$ is the reflectivity of the diamond-air interface. The derivations of Eq. (2) and (3) are provided in the Supplementary Data. All measured signals were averaged over the 550-650 nm spectral range, where the reflectivity of the reference mirror is well-characterized (~0.985-0.995), allowing for precise measurements of the probe intensity impinging on the upstream diamond-air interface. Eq. (2) and (3) contain only two unknowns ($R_{dia\text{-}smp}$ and T) and are solved simultaneously. Two of the three sets of roots included imaginary $R_{dia\text{-}smp}$ and T and were discarded. Using $R_{dia\text{-}smp}$ from the real set of roots, we solve Eq. (1) for n_{smp}, the refractive index of ferropericlase at 600 nm (because of the averaging of $\frac{I_1+I_2}{I_0}$ and T over 550-650 nm). In solving

Eq. (1), we assume a pressure-independent refractive index of diamond (n_{dia} = 2.418 (Hynes, 2016)). The validity of this assumption and possible effects of a pressure dependence of n_{dia} have been discussed in detail by Schifferle et al. (2022). Their results on MgO support the hypothesis n_{dia} = *constant*. However, we provide all necessary data for the evaluation of n_{smp} in **Supplementary Table 1** which can be reanalyzed when more detailed information on the pressure-dependence of n_{dia} is available. The solutions to Eq. (1-3) have been found with Python SciPy and SymPy libraries (Meurer et al., 2017; Walt et al., 2011). We independently tested the reflectivity method for semitransparent samples developed in this work by reproducing the high-pressure evolution of the refractive index of an Fe-bearing basaltic glass (*i.e.* absorbing in the visible) reported by Kuryaeva and Kirkinskii (1997). We empirically estimate the overall uncertainty in the measured n_{smp} at ~1%. The effect of uniaxial stress (due to the lack of pressure-transmitting medium) on the measured index is likely smaller than the overall experimental uncertainty because the pressure dependence of the refractive index of MgO (and ferropericlase) is small. That is, moderate pressure gradients across the sample chamber (*e.g.,* of 5 %) would cause index gradient with the total difference at the sample center and periphery of << 1%. This is further supported by first-principles simulations: e.g., the pressure-dependence of the refractive index of MgO measured in the DAC with the same method as used in the present work is in excellent agreement with DFT computations (Schifferle et al., 2022).

DOI: https://doi.org/10.2138/am-2023-9100. http://www.minsocam.org/

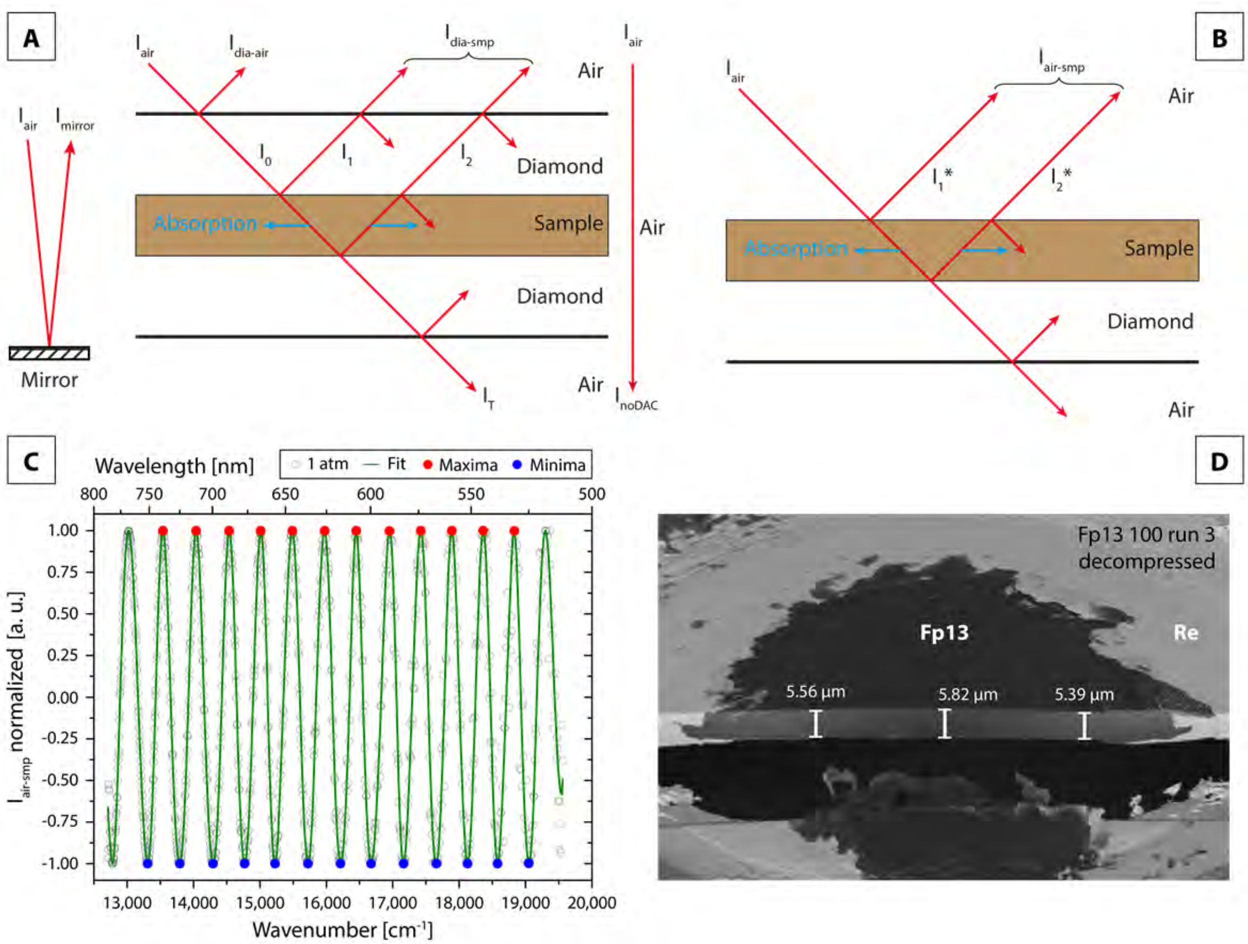

Figure 1: **A**: Reflectivity measurements in a partially absorbing sample at high-pressure conditions. The perpendicularly-incident probe laser is partially reflected at the air-mirror, diamond-air and diamond-sample interfaces. Oblique probe incidence is depicted for clarity. **B**: Reflectivity measurements for the decompressed sample in an opened diamond anvil cell. **C**: A normalized intensity spectrum of Fp13 (run 3) decompressed to 1 atm. The local extrema (blue and red circles) served to find the optical path ($n_{1atm}d_{1atm}$), where d_{1atm} is sample thickness. **D**: A secondary electron microscope image of a focused ion beam cross-section of the of Fp13 (run 3) decompressed to 1 atm used to directly image the sample thickness. The light grey part is the Re gasket and dark grey is Fp13.

We also measured the refractive index of Fp13 decompressed to 1 atm after one of the DAC runs. To this end, we removed the upper diamond anvil to ensure no pressure was applied to the sample and measured the reflectivity of the air-sample interface where $I_{air-smp}$ is composed of I_1* and I_2*, which are individual reflections from the air-sample and sample-diamond interfaces (**Figure 1 B**). The normalized reflectance spectrum was analyzed for the average spectral separation of the interference fringes to obtain the optical path ($OP = n_{1atm}d_{1atm}$) (**Figure 1 C**). A radial cross-section through the retrieved sample (**Figure 1**, **D**) cut by a focused ion beam allowed to directly measure the thickness of decompressed ferropericlase at the center of the DAC sample cavity (d_{1atm}) and to obtain the refractive index of Fp13 as $n_{1\,atm} = \frac{OP}{d_{1atm}}$.

Dispersion analysis

The interference fringe spectra can be analyzed for the wavelength-dispersion of the refractive index following (Schifferle et al., 2022) (for more details, see their section 2.3). Briefly, for each extremum the interference condition is:

$$\lambda k(\lambda) = 2dn_{smp}(\lambda) \quad \text{(Eq. 4)},$$

where $k(\lambda)$, is the interference order number of the minimum/maximum (half-integer step size) observed at the wavelength λ, d is sample thickness at high pressure, and $n_{smp}(\lambda)$ is the refractive index at the extremum. Using Eq. 4 for each pair of extrema we estimated sample thickness assuming n_{smp} is wavelength independent, which is accurate within ~1 % for Fe-poor Fp because the index dispersion of MgO across the studied spectral range is small (~1 %) (Stephens and Malitson, 1952). We will provide evidence below that the index dispersion of Fp13 is indeed comparable to MgO. The sample thickness averaged over all used extrema pairs is then used to assign the interference order number to the extremum closest to 600 nm (e.g., k_{600nm} = 70 at 16.9 GPa, k_{600nm} = 41.5 at 109.1 GPa) and subsequently to all the other observed extrema. Finally, the refractive index at each λ is calculated using Eq. 4 for all the observed extrema. The propagation of random and systematic relative errors in the measured index dispersion yields overall errors of ~0.9% at ~23 GPa and ~2.6% at ~109 GPa. The increase in this error is likely due to diamond cupping at high pressure (Schifferle et al., 2022).

Computation of refractive index and index dispersion for MgO and ferropericlase

Atomistic model calculations were carried out within the framework of DFT (Hohenberg and Kohn, 1964) and the pseudopotential method using the CASTEP simulation package (Clark et al., 2005). Ultrasoft pseudopotentials were generated "on the fly" using the parameters provided with the CASTEP distribution. These pseudopotentials have been extensively tested for accuracy and transferability (Perdew et al., 1996). The pseudopotentials were employed in conjunction with plane waves up to a kinetic energy cutoff of 630 eV (Lejaeghere et al., 2016). Spin-polarised calculations were carried out with the PBE exchange-correlation functional and a Hubbard U of 2.5 eV for the Fe-*d*-states. As spin-polarized DFT-GGA-PBE + U calculations of low symmetry structures (such as MgO with Fe defects) are computationally expensive, the calculations here were limited to 64-atom supercells. In such a cell, a single Fe-atom is about 8.5 Å away from the next Fe atom, and hence interactions between Fe atoms are small. Increasing the concentration of Fe atoms, e.g. by placing a second Fe Atom in this simulation cell, would then have to consider the numerous relative arrangements, possible clustering and Fe-Fe interactions. Using a larger simulation cell or studying Fe-Fe interactions in the 8.5 Å cell were beyond the scope of the present study. Monkhorst-Pack grids (Monkhorst and Pack, 1976) were used for Brillouin zone

DOI: https://doi.org/10.2138/am-2023-9100. http://www.minsocam.org/

integrations with a distance of < 0.029 $Å^{-1}$ between grid points. Convergence criteria included an energy change of < 5×10^{-6} eV/atom, a maximal force of < 0.01 eV/Å, and a maximal deviation of the stress tensor < 0.02 GPa from the imposed stress tensor. All calculations were carried out in the athermal limit, *i.e.*, the influences of temperature and zero-point motion were not taken into account.

3. RESULTS AND DISCUSSION

The refractive indices of Fp13 and Fp24 measured in this work are shown in **Figure 2**. At all pressures, the index of Fp24 at 600 nm is ~1-2 % higher than that of Fp13, consistent with the results of Henning et al. (1995) who measured the optical properties of $Fe_xMg_{1-x}O$ (x = 0.4-1) at 1 atm. The indices of both Fp13 and Fp24 increase with pressure with no sharp discontinuity over the expected spin transition range of 40-80 GPa (Glazyrin et al., 2016; Kantor et al., 2009; Lin et al., 2006). In one of the runs (Fp13, run3), the index measured at 600 nm appears ~1% too low than what may be expected from its value independently measured at 1 atm as well as expected from the results of Henning et al. (1995). It is plausible that submicron impurities are present in that loading which contributed an up-shift to the measured $\frac{I_1+I_2}{I_0}$ through light back scattering, increasing the apparent $R_{dia\text{-}smp}$ and thus decreasing n_{smp}. This is indirectly supported by our data on Fp24, which remained fully opaque upon compression, in which case the evaluation of $R_{dia\text{-}smp}$ is more accurate because only the upstream diamond-sample reflection (I_1) contributes to $\frac{I_1+I_2}{I_0}$ at $T = 0$ (see Eq. 2). At $P > 60$ GPa, the increase in refractive indices of Fp13 (+0.0014 ($\pm1.31\times10^{-3}$) per 10 GPa) and Fp24 (+0.0021 ($\pm7.75\times10^{-4}$) per 10 GPa) is small, but resolvable within the uncertainty of our determination; the refractive index of mantle-like Fp is not independent of pressure (dashed lines in **Figure 2**). The extrapolation of the high-pressure index of Fp24 at 600 nm to 1 atm is in excellent agreement with the expectation from the literature (Henning et al., 1995).

DOI: https://doi.org/10.2138/am-2023-9100. http://www.minsocam.org/

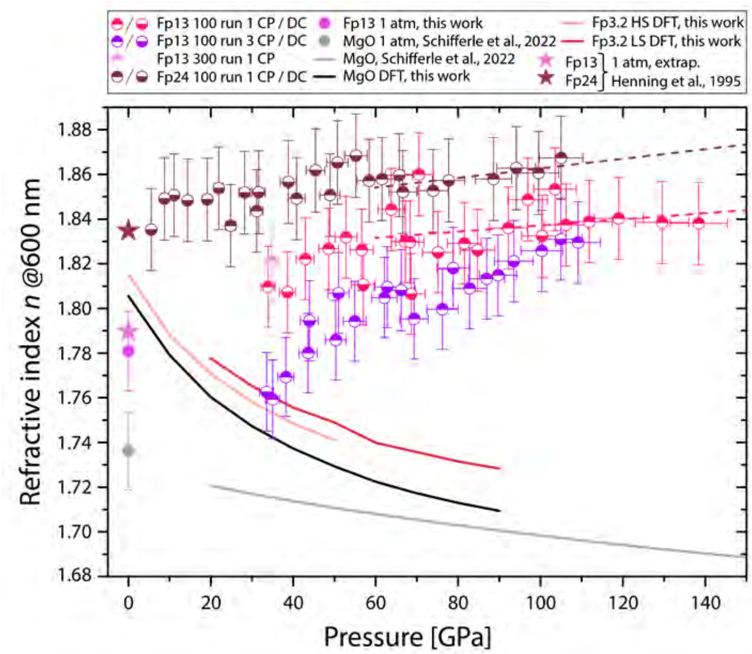

Figure 2 The refractive index of Fp13 and Fp24 at 600 nm measured in this work, compared to DFT calculations of Fp3.2 (high- and low-spin) and MgO, as well as experimental data on MgO from Schifferle et al. (2022). Stars represent extrapolations based on the indices of iron-rich Fp reported by Henning et al. (1995) (at 1 atm). Red (Fp13) and magenta (Fp24) dashed lines are visual guides based on a linear *dn*/*dP* fit for to our data at P > 60 GPa. Abbreviations: CP = compression, DC = decompression.

The refractive index of ferropericlase is considerably higher than that of MgO (**Figure 2**) because of the higher polarizability of Fe^{2+} compared to Mg^{2+} at 1 atm ($^{[6]}Fe^{2+}$ 2.040 Å^3, $^{[6]}Mg^{2+}$ 0.651 Å^3 (Shannon and Fischer, 2016)). This results in a compositional dependence of the refractive index of ferropericlase (higher Fe content leads to higher index, Supplementary **Figure S1**). Interestingly, while the pressure-derivatives of the indices of Fp13 and Fp24 are positive, that of MgO is negative (Balzaretti and Da Jornada, 1990; Fratanduono et al., 2013; Oganov et al., 2003; Schifferle et al., 2022). The increase in refractive index with pressure entails that the Lorenz-Lorentz factor $(\frac{n^2-1}{n^2+2} \propto \frac{\rho}{\alpha_{LL}})$ also increases with pressure (ρ is density, α_{LL} is Lorenz-Lorentz polarizability). Accordingly, we attribute the positive pressure-dependence of the refractive index of ferropericlase to its anomalous polarizability (compared to MgO; Supplementary **Figure S2**), because the compressibility of MgO, Fp13, and Fp24 are similar. However, our DFT computations indicate that at low Fe^{2+} concentrations (Fp3.2) the pressure-derivative of the refractive index is similar to that of MgO (see black and grey lines in **Figure 2**). We note that Fe-Fe interactions, which are very weak or absent in our DFT computations as the Fe-Fe-distances are large (1 Fe, 31 Mg atoms in the supercell), are likely present in Fp13 and Fp24 because their Fe content exceeds the percolation limit (12% (Lorenz and Ziff, 1998)). Above the percolation limit, an interconnected network of overlapping t_{2g} orbitals between adjacent edge-sharing FeO_6 octahedra is present. We propose that pressure-induced electron delocalization along the interatomic t_{2g}-t_{2g} joints (Diamond et al., 2022) maintains higher polarizability in Fp and is thus the reason for the anomalous positive pressure-dependence of the refractive indices of HS Fp13 and Fp24. Such electron delocalization is complete in the LS state; hence, the refractive index of LS Fp is almost pressure independent (*i.e.*, MgO-like).

We used the high-pressure refractive index and the interferometric data to obtain d, the thickness of ferropericlase at high pressure. To avoid fluctuations in d due to the apparently random error in the index, n is derived from a linear P vs. n fit (see Supplementary Data). Please note, that possible pressure differences across the sample were not considered because pressure differences at the sample center and periphery were not resolvable within the uncertainty of the pressure determination method (5% relative). Such moderate pressure gradients across the sample chamber would cause index gradient with the total difference at the sample center and periphery of << 1%. This implies that the differences in optical path measured at the center and periphery of the sample chamber (which may be as high as 2-3 %) are primarily due to differences in sample thickness. Next, we quantify the absorption coefficient of ferropericlase as: $\alpha(600\,nm) = A \cdot \ln(10)/d$, where $A = -log_{10}T$ is the measured optical absorbance of the sample (T is transmission). Please note that even at low pressure (< 30 GPa) transmission data and the interference fringe pattern quality were sufficient to obtain accurate thicknesses (the variation in optical path inferred for different fringes is less than 1%) and absorption coefficients (3% error). Due to the high absorption coefficient of Fp24, transmission could only be detected in very thin samples (< 6 μm), achieved only on decompression as samples in DACs continue to thin upon pressure release (Lobanov and Geballe, 2022). Here we extend this seemingly general behavior to ferropericlase (Supplementary **Figure S3**), and show that thickness estimations based on the assumption of isotropic compression severely overestimate the real sample thickness by up to ~50%, similar to the conclusion of (Lobanov and Geballe, 2022). A similar gasket thinning on decompression has also been noted previously by Dewaele et al. (2003) with He as a sample, albeit the gasket thickness and the maximum pressure were very different (~48 μm at ~20 GPa). These suggest that sample size and hardness likely play a role in the gasket thinning upon decompression.

For Fp13 we find α(600 nm) to increase from 20 GPa up to ~57 GPa by a factor of ~3, where the maximum is reached at ~2000 cm^{-1} (**Figure 3**). For the pressure range > 57 to ~85 GPa we find a sharp decrease in α(600 nm) by ~30%. At P > 85 GPa, the absorption coefficient reaches a plateau at ~1300 cm^{-1}. The pressure range of the negative $d\alpha/dP$ suggests that the decrease of α is related to the spin transition in Fp13 (Schifferle and Lobanov, 2022). In HS Fp, the transition energy of the single multiplicity allowed crystal field (*d-d*) band ($^5T_{2g} \rightarrow {^5E_g}$) is almost pressure independent (Keppler et al., 2007; Schifferle and Lobanov, 2022); thus, this band does not contribute to the increase in the absorption coefficient up to 60 GPa. One of the *d-d* bands of LS Fp appears close to 600 nm (16,667 cm^{-1}) at ~60 GPa (Schifferle and Lobanov, 2022) and would only increase the absorption coefficient, in contrast to what is observed. At the same time, the absorption edge shows a qualitative red-shift (in HS) and blue-shift (in LS) with pressure (Goncharov et al., 2006; Keppler et al., 2007; Schifferle and Lobanov, 2022). We

DOI: https://doi.org/10.2138/am-2023-9100. http://www.minsocam.org/

conclude, therefore, that the trend in α(600 nm) is mostly related to the intensity of the UV-absorption edge in ferropericlase with a minor contribution of the crystal field bands.

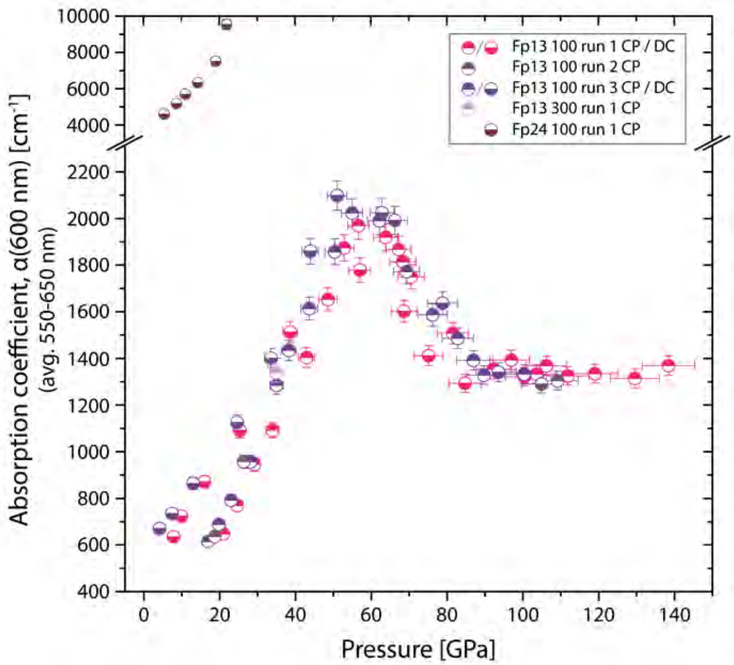

Figure 3 Absorption coefficients of Fp13 and Fp24 at 600 nm based on direct measurements of the optical path ($n_{smp}d$). Thicknesses used for the calculation of the absorption coefficient are obtained by dividing the optical path by n_{smp} at 600 nm and neglecting the index dispersion in the analyzed spectral range (~500-800 nm) which is ~1% or less (see discussion in the main text). The uncertainty in d is that of refractive index and is ~1%. Please note the break in y-axis. Abbreviations: CP = compression, DC = decompression.

The variation of α(600 nm) with pressure is reversible upon decompression down to ~40 GPa. Our α(600 nm) allows to derive the wavelength-dependent absorption coefficients (and thus the imaginary part of the refractive index) from previously published absorbance data for the same Fp13 sample (Schifferle and Lobanov, 2022) (Supplementary **Figure S4**). Compared to previous reports on the absorption coefficient of ferropericlase where the sample thickness at high pressure was estimated using its equation of state (Lobanov et al., 2021), we show that α is lower by up to ~50%. This is because Lobanov et al. (2021) measured the thickness of their Fp13 sample after decompression and assumed the sample was thinner at high pressure. As show by Lobanov and Geballe (2022) samples in DACs continue to thin upon decompression; and their data can be used to revise the Fp13 absorption coefficients reported in Lobanov et al. (2021). An approximate correction suggests that the radiative thermal conductivity of ferropericlase at the base of the mantle has been underestimated by roughly a factor of two in that previous study.

Concomitantly to the directly measured decrease in the absorption coefficient by ~30 % at 57-85 GPa, we observe a sharp decrease in the absolute wavelength dispersion of the refractive index of Fp13 (**Figure 4**). Below ~40 GPa, the wavelength-dispersion of the refractive index of Fp13 is essentially pressure independent. At P = 43.6-69.3 GPa, however, the index dispersion is dramatically decreased by a factor of ~3 from ~0.0174 (± ~1 %) to 0.006 (± ~2 %) (orange line, **Figure 4, A**). Yet, at $P > 69.3$ GPa, the absolute index dispersion is almost restored at ~0.016 (±1 %) (**Figure 4, B**). The index dispersion is ~50 % stronger in HS and LS Fp13 than in MgO, which is qualitatively consistent with our DFT computations that produced ~20 % higher dispersion in the case of Fp3.2 than in the case of pure MgO. Likewise, our computations support the notion that the index dispersion in HS and LS Fp3.2 are similar. In contrast to pure HS and LS ferropericlase probed in experiments and computations, the measured index dispersion of MS Fp13 is anomalously low: ~50 % lower than that of MgO at 60-80 GPa. We note, that the dispersion data is analyzed assuming a constant refractive index at 600 nm of 1.79 (based on the expectation for Fp13 at 1 atm (Henning et al., 1995) to better account for deviations due to random errors in the refractive index. This, however, does not significantly affect the inferred index dispersion, because possible differences in refractive index at 600 nm of 2-3 % result mostly in a vertical shift of the index dispersion curve and not its slope (**Figure 4 A**).

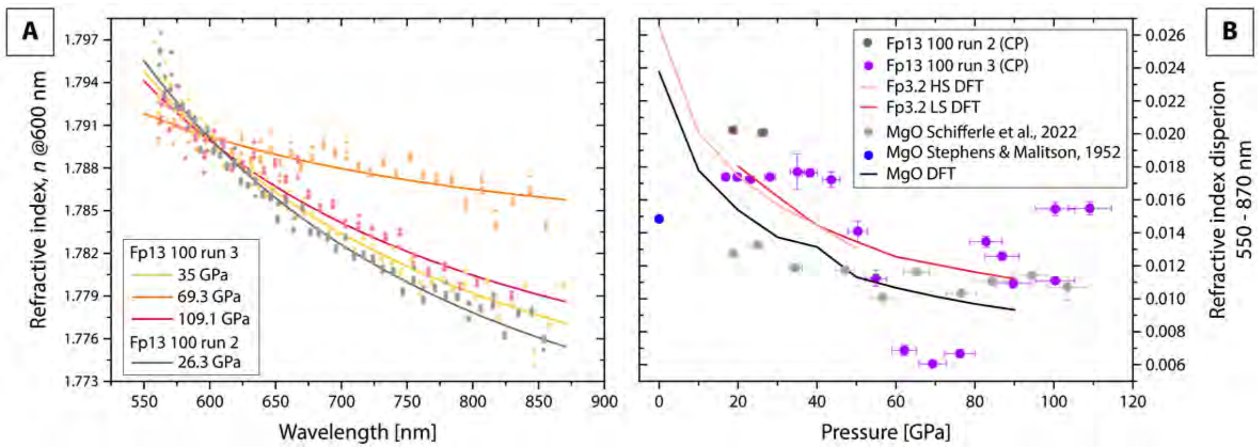

Figure 4 (**A**) Dispersion of the refractive index of Fp13 (compression) at selected pressures (assuming a pressure-independent refractive index n(600 nm) of 1.79) and (**B**) as the difference between refractive indices at 550 and 870 nm compared to DFT calculations for Fp3.2 and MgO as well as previously published experimental data (Schifferle et al., 2022; Stephens and Malitson, 1952).

We analyzed the dispersion by the single-effective-oscillator model of Wemple and DiDomenico (1971). In this model, the wavelength dependence of the refractive index is related to two fitting parameters E_0 and E_d, which describe the single oscillator energy and dispersion energy (in eV), respectively. These quantities are related to the band gap width and bonding environment:

$$n(\lambda) = \sqrt{\frac{E_d \cdot E_0}{E_0^2 - \left(\frac{h \cdot c}{\lambda}\right)^2} + 1} \qquad \text{(Eq. 4)}$$

Here, h is the Planck's constant in eV·s and c the speed of light in m/s and λ the wavelength in m. By fitting Eq. (4) to the measured index dispersion at 550-870 nm, we find E_d and E_0. An in-detail description of the procedure can be found in Schifferle et al. (2022).

Wemple and DiDomenico (1971) proposed that E_0 is related to the average optical band gap, and that the ratio $E_0/1.5$ approximates independently measured band gaps. The denominator in this ratio, however, is material dependent. To estimate it for Fp13 we performed a Tauc plot analysis of the low-pressure optical absorption data of Fp13 reported in Schifferle and Lobanov (2022), which yields the minimum band gap energy of 2.75 eV. We thus divide all fitted E_0 by 3.8 to match 2.75 eV at low pressure (*i.e.* at $P < \sim 40$ GPa, where the wavelength-dispersion is essentially pressure-independent). Although the values of $E_0/3.8$ at $P < 40$ GPa are broadly consistent with previous DFT calculations (Holmstrom and Stixrude, 2015; Hsu and Wentzcovitch, 2014; Li and Wang, 2015; Song et al., 2019; Sun et al., 2022), our results likely underestimate the band gap as broad-range UV spectra are not available. Despite these uncertainties, we can derive semi-quantitative trends in band gap energy.

In **Figure 5** we show $E_0/3.8$ and $E_d/7.6$ (for illustration only, *i.e.,* to scale E_d close to $E_0/3.8$) of Fp13 from the Wemple and DiDomenico (1971) single-effective oscillator analysis and compare it with existing computations of the optical band gap in ferropericlase. Regardless of the chosen scaling factor for E_0, our experimental data (**Figure 5**) suggests a constant band gap energy up to ~40 GPa. In the MS state ($P \approx 50$-80 GPa), we observe an increase in $E_0/3.8$ with a maximum at ~69.3 GPa of ~4.7 eV. This peak in the band gap probably represents 50% HS and 50% LS, consistent with the LS fraction inferred by Mössbauer spectroscopy (Kantor et al., 2009). At $P > 100$ GPa, the band gap energy is comparable to that at $P < 40$ GPa. These semi-quantitative insights into the band gap energy are consistent with DFT computations (Song et al., 2019; Sun et al., 2022), which suggest a pressure-independent band gap energy for high- and low-spin states. The possible intermediate spin (IS) state, although energetically disfavored (Hsu and Wentzcovitch, 2014), also does not deviate from the general trend of a near-constant band gap in DFT calculations. However, to the best of our knowledge, there are no DFT computations of the MS state available, which we probed optically here for the first time. E_d shows a trend qualitatively similar to that of E_0. Because E_d represents the distribution of charge around the anion (Wemple and DiDomenico, 1971), its increase and decrease over the spin transition might reflect the decrease/increase in *p-d* orbital overlap. For example, charge donation from oxygen to the empty e_g orbitals in the LS state has been inferred from the decrease in the Fe-O bond covalency (Schifferle and Lobanov, 2022). A similar ligand-to-Fe donation has been proposed as a consequence of the Fe^{2+} HS to LS transition in S- and Sn-thiospinels (Womes and Jumas, 2013).

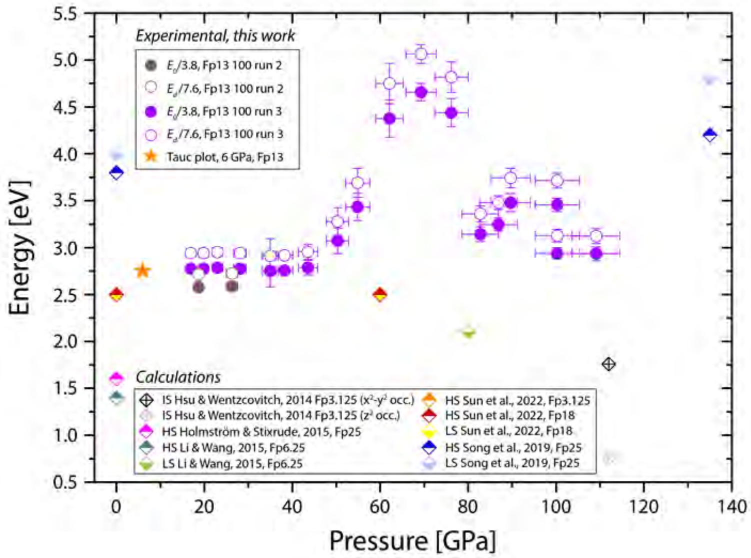

Figure 5 Results of the Wemple and DiDomenico (1971) fit (E_0/3.8 and E_d/7.6) to the measured index dispersion of Fp13 (circles). Orange star represents the band gap estimation based on Tauc plot analysis (Tauc, 1968) of data from Schifferle and Lobanov (2022). In addition, we show calculations from literature for the band gap in different ferropericlase compositions and spin configurations (diamonds). Abbreviations: high-spin (HS), intermediate-spin (IS) and low-spin (LS). Please note, datapoints from Sun et al. (2022) for the three spin configurations are directly overlapping at 0 GPa and 2.5 eV (HS Fp 3.125, HS Fp18 and LS Fp18) as well as at 60 GPa and 2.5 eV (HS Fp18, LS Fp18).

The increase in E_0/3.8 by ~1.95 eV and the reduction of the absorption coefficient by ~35% over the spin transition range offers a qualitative understanding of the previously reported drop of electrical conductivity by a factor of up to three in ferropericlase at ~50-70 GPa (Lin et al., 2007; Ohta et al., 2007). In contrast to these previous studies, where a lower small polaron mobility and/or density in LS ferropericlase was proposed as an explanation (Lin et al., 2007; Ohta et al., 2007), our data suggests that lower electron mobility is characteristic of the MS state while that in HS and LS is similar. We propose that qualitatively this can be understood in terms of small polaron transport through the crystal lattice, which requires electron exchange between adjacent Fe sites: $Fe^{2+} \xrightarrow{e^-} Fe^{2+} = Fe^{3+} + Fe^{+}$. In particular, the absorption coefficient of Fp may be strongly enhanced due to magnetic coupling between adjacent iron sites, which offers an efficient means of relaxing the spectroscopic selection rules, as has been shown for Fe^{3+}-O_6 octahedra (Sherman and Waite, 1985). Considering that magnetic collapse is a defining characteristic of LS Fe^{2+} (Cohen et al., 1997), the magnetic relaxation of spectroscopic selection rules is only possible in HS-HS pairs. The collapse of magnetic moments of individual Fe atoms in the MS and LS states is thus a viable explanation for the ~30% decrease of the absorption coefficients at P > 57 GPa. This mechanism, however, does not explain the relatively high refractive index dispersion of the LS Fp.

4. IMPLICATIONS

A strong reduction of the electrical conductivity of MS ferropericlase opens a new scenario for the overall conductivity of the lowermost mantle. *Ab initio* computations indicate that ferropericlase is predominantly in the mixed spin state at depths greater than ~1900 km and down to the core-mantle boundary at ~2900 km because of the high temperatures of the lower mantle, which broaden the mixed spin pressure range (Holmstrom and Stixrude, 2015). If the drop in electrical conductivity at ~50-70 GPa is due to the lower small polaron mobility/density in LS Fp as proposed by Lin et al. (2007) and Ohta et al. (2007), then one expects only a moderate drop in mantle conductivity if any at depths >1900 km, because LS Fp is never dominant even at the base of the mantle. In contrast, if the drop in Fp conductivity is indeed characteristic of the MS state (as inferred in this work), then one expects a significant reduction of mantle electrical conductivity over the lowermost 1000 km of the mantle. The magnetic data recorded by SWARM, which is a low-orbit satellite mission dedicated to the study of Earth's magnetic field, now allows 3D mapping the conductivity of the Earth's mantle down to ~2000 km depth (Kuvshinov et al., 2021; Velimsky and Knopp, 2021). Deeper conductivity models will be enabled by the continuing geomagnetic observations and may thus be sensitive to the changes in conductivity due to the spin crossover in ferropericlase. Yet another alternative is that small polaron is a relatively unimportant mechanism in the lower mantle because of the crossover to the large polaron mechanism at $T > \sim 1000$ K, as suggested by earlier studies at $P < \sim 30$ GPa (Dobson and Brodholt, 2000; Dobson et al., 1997). A transition to a band conduction mechanism in Fp at $T > \sim 2000$ K has been proposed by theoretical computations (Holmstrom et al., 2018), consistent with the results of optical experiments at high *P-T* that indicate a crossover to opaque Fp at $T >$ 2500 K (Lobanov et al., 2021). Direct measurements of Fp electrical conductivity at realistic lower mantle *P-T* conditions are thus needed to improve our understanding of lower mantle conductivity.

ACKNOWLEDGEMENTS

This work was supported by the Helmholtz Young Investigators Group CLEAR (VH-NG-1325). We thank Brent Grocholski, and Leonid Dubrovinsky for donating ferropericlase samples (Fp13 and Fp24 in this order) and specifically Caterina Melai for the synthesis of Fp24. We are grateful to Anja Schreiber for her technical support with thickness measurements of the decompressed sample. BW is grateful for support through the BIOVIA Science ambassador program.

REFERENCES

Akahama, Y., and Kawamura, H. (2006) Pressure calibration of diamond anvil Raman gauge to 310 GPa. Journal of Applied Physics, 100(4), 043516.

Alexandrescu, M.M., Gibert, D., Le Mouel, J.L., Hulot, G., and Saracco, G. (1999) An estimate of average lower mantle conductivity by wavelet analysis of geomagnetic jerks. Journal of Geophysical Research-Solid Earth, 104(B8), 17735-17745.

Aprilis, G., Pakhomova, A., Chariton, S., Khandarkhaeva, S., Melai, C., Bykova, E., Bykov, M., Fedotenko, T., Koemets, E., McCammon, C., and others. (2020) The Effect of Pulsed Laser Heating on the Stability of Ferropericlase at High Pressures. Minerals, 10(6), 542.

Balzaretti, N.M., and Da Jornada, J.A.H. (1990) Volume dependence of the electronic polarizability of magnesium oxide. High Pressure Research, 2(3), 183-191.

Bloxham, J., and Jackson, A. (1992) Time-Dependent Mapping of the Magnetic-Field at the Core-Mantle Boundary. Journal of Geophysical Research-Solid Earth, 97(B13), 19537-19563.

Buffett, B.A. (2015) 8.08 - Core–Mantle Interactions A2 - Schubert, Gerald. In G. Schubert, Ed. Treatise on Geophysics (Second Edition), p. 213-224. Elsevier, Oxford.

Clark, S.J., Segall, M.D., Pickard, C.J., Hasnip, P.J., Probert, M.J., Refson, K., and Payne, M.C. (2005) First principles methods using CASTEP. Zeitschrift Fur Kristallographie, 220(5-6), 567-570.

Cohen, R.E., Mazin, I.I., and Isaak, D.G. (1997) Magnetic collapse in transition metal oxides at high pressure: Implications for the Earth. Science, 275(5300), 654-657.

Constable, S. (2015) 5.07 - Geomagnetic Induction Studies. In G. Schubert, Ed. Treatise on Geophysics (Second Edition), p. 219-254. Elsevier, Oxford.

Dewaele, A., Eggert, J.H., Loubeyre, P., and Le Toullec, R. (2003) Measurement of refractive index and equation of state in dense He, H_2, H_2O, and Ne under high pressure in a diamond anvil cell. Physical Review B, 67(9), 094112.

Diamond, M.R., Shen, G.Y., Popov, D.Y., Park, C., Jacobsen, S.D., and Jeanloz, R. (2022) Electron Density Changes across the Pressure-Induced Iron Spin Transition. Physical Review Letters, 129(2).

Dobson, D.P., and Brodholt, J.P. (2000) The electrical conductivity of the lower mantle phase magnesiowustite at high temperatures and pressures. Journal of Geophysical Research-Solid Earth, 105(B1), 531-538.

Dobson, D.P., Richmond, N.C., and Brodholt, J.P. (1997) A high-temperature electrical conduction mechanism in the lower mantle phase $(Mg,Fe)_{1-x}O$. Science, 275(5307), 1779-1781.

Duan, P.S., and Huang, C.L. (2020) Intradecadal variations in length of day and their correspondence with geomagnetic jerks. Nature Communications, 11(1).

Fratanduono, D.E., Eggert, J.H., Akin, M.C., Chau, R., and Holmes, N.C. (2013) A novel approach to Hugoniot measurements utilizing transparent crystals. Journal of Applied Physics, 114(4), 043518.

Glazyrin, K., Miyajima, N., Smith, J.S., and Lee, K.K.M. (2016) Compression of a multiphase mantle assemblage: Effects of undesirable stress and stress annealing on the iron spin state crossover in ferropericlase. Journal of Geophysical Research-Solid Earth, 121(5), 3377-3392.

DOI: https://doi.org/10.2138/am-2023-9100. http://www.minsocam.org/

Goncharov, A.F., Struzhkin, V.V., and Jacobsen, S.D. (2006) Reduced radiative conductivity of low-spin (Mg,Fe)O in the lower mantle. Science, 312(5777), 1205-1208.

Hansen, K.W., and Cutler, I.B. (1966) Electrical Conductivity in $Fe_{1-x}O$-MgO Solid Solutions. Journal of the American Ceramic Society, 49(2), 100-102.

Henning, T., Begemann, B., Mutschke, H., and Dorschner, J. (1995) Optical properties of oxide dust grains. Astronomy & Astrophysics Supplement Series, 112(1), 143-149.

Hohenberg, P., and Kohn, W. (1964) Inhomogeneous Electron Gas. Physical Review, 136(3B), B864-B871.

Holme, R., and de Viron, O. (2013) Characterization and implications of intradecadal variations in length of day. Nature, 499(7457), 202-205.

Holmstrom, E., and Stixrude, L. (2015) Spin crossover in ferropericlase from first-principles molecular dynamics. Physical Review Letters, 114(11), 117202.

Holmstrom, E., Stixrude, L., Scipioni, R., and Foster, A.S. (2018) Electronic conductivity of solid and liquid (Mg, Fe)O computed from first principles. Earth and Planetary Science Letters, 490, 11-19.

Hsu, H., and Wentzcovitch, R.M. (2014) First-principles study of intermediate-spin ferrous iron in the Earth's lower mantle. Physical Review B, 90(19), 195205.

Hynes, W.M. (2016) CRC Handbook of Chemistry and Physics. CRC Press, Boca Raton; London; New York.

Irifune, T., Shinmei, T., McCammon, C.A., Miyajima, N., Rubie, D.C., and Frost, D.J. (2010) Iron Partitioning and Density Changes of Pyrolite in Earth's Lower Mantle. Science, 327(5962), 193-195.

Iyengar, G.N.K., and Alcock, C.B. (1970) A study of semiconduction in dilute magnesio-Wüstites. The Philosophical Magazine: A Journal of Theoretical Experimental and Applied Physics, 21(170), 293-304.

Kantor, I., Dubrovinsky, L., McCammon, C., Steinle-Neumann, G., Kantor, A., Skorodumova, N., Pascarelli, S., and Aquilanti, G. (2009) Short-range order and Fe clustering in $Mg_{1-x}Fe_xO$ under high pressure. Physical Review B, 80(1).

Keppler, H., Kantor, I., and Dubrovinsky, L.S. (2007) Optical absorption spectra of ferropericlase to 84 GPa. American Mineralogist, 92(2-3), 433-436.

Kuryaeva, R.G., and Kirkinskii, V.A. (1997) Influence of high pressure on the refractive index and density of tholeiite basalt glass. Physics and Chemistry of Minerals, 25(1), 48-54.

Kuvshinov, A., Grayver, A., Tofner-Clausen, L., and Olsen, N. (2021) Probing 3-D electrical conductivity of the mantle using 6 years of Swarm, CryoSat-2 and observatory magnetic data and exploiting matrix Q-responses approach. Earth Planets and Space, 73(1).

Lejaeghere, K., Bihlmayer, G., Bjorkman, T., Blaha, P., Blugel, S., Blum, V., Caliste, D., Castelli, I.E., Clark, S.J., Dal Corso, A., and others. (2016) Reproducibility in density functional theory calculations of solids. Science, 351(6280), 1415.

Li, H.Y., and Wang, Q.B. (2015) The electronic properties of ferropericlase under pressure calculated by first principles. Proceedings of the First International Conference on Information Sciences, Machinery, Materials and Energy (Icismme 2015), 126, 730-733.

Li, X.Y., and Jeanloz, R. (1990) High Pressure-Temperature Electrical-Conductivity of Magnesiowustite as a Function of Iron-Oxide Concentration. Journal of Geophysical Research-Solid Earth and Planets, 95(B13), 21609-21612.

This is the peer-reviewed, final accepted version for American Mineralogist, published by the Mineralogical Society of America.
The published version is subject to change. Cite as Authors (Year) Title. American Mineralogist, in press.
DOI: https://doi.org/10.2138/am-2023-9100. http://www.minsocam.org/

Lin, J.F., Gavriliuk, A.G., Struzhkin, V.V., Jacobsen, S.D., Sturhahn, W., Hu, M.Y., Chow, P., and Yoo, C.S. (2006) Pressure-induced electronic spin transition of iron in magnesiowustite-(Mg,Fe)O. Physical Review B, 73(11), 113107.

Lin, J.F., Weir, S.T., Jackson, D.D., Evans, W.J., Vohra, Y.K., Qiu, W., and Yoo, C.S. (2007) Electrical conductivity of the lower-mantle ferropericlase across the electronic spin transition. Geophysical Research Letters, 34(16), L16305.

Lobanov, S.S., and Geballe, Z.M. (2022) Non-Isotropic Contraction and Expansion of Samples in Diamond Anvil Cells: Implications for Thermal Conductivity at the Core-Mantle Boundary. Geophysical Research Letters, 49(19), e2022GL100379.

Lobanov, S.S., Soubiran, F., Holtgrewe, N., Badro, J., Lin, J.-F., and Goncharov, A.F. (2021) Contrasting opacity of bridgmanite and ferropericlase in the lowermost mantle: Implications to radiative and electrical conductivity. Earth and Planetary Science Letters, 562, 116871.

Lobanov, S.S., and Speziale, S. (2019) Radiometric Temperature Measurements in Nongray Ferropericlase With Pressure- Spin- and Temperature-Dependent Optical Properties. Journal of Geophysical Research: Solid Earth, 124, 12825-12836.

Lobanov, S.S., Speziale, S., Winkler, B., Milman, V., Refson, K., and Schifferle, L. (2022) Electronic, Structural, and Mechanical Properties of SiO_2 Glass at High Pressure Inferred from its Refractive Index. Physical Review Letters, 128(7), 077403.

Longo, M., McCammon, C.A., and Jacobsen, S.D. (2011) Microanalysis of the iron oxidation state in (Mg,Fe)O and application to the study of microscale processes. Contributions to Mineralogy and Petrology, 162(6), 1249-1257.

Lorenz, C.D., and Ziff, R.M. (1998) Precise determination of the bond percolation thresholds and finite-size scaling corrections for the sc, fcc, and bcc lattices. Physical Review E, 57(1), 230-236.

Meurer, A., Smith, C.P., Paprocki, M., Certik, O., Kirpichev, S.B., Rocklin, M., Kumar, A., Ivanov, S., Moore, J.K., Singh, S., and others. (2017) SymPy: symbolic computing in Python. Peerj Computer Science, e103.

Monkhorst, H.J., and Pack, J.D. (1976) Special points for Brillouin-zone integrations. Physical Review B, 13(12), 5188-5192.

Oganov, A.R., Gillan, M.J., and Price, G.D. (2003) Ab initio lattice dynamics and structural stability of MgO. Journal of Chemical Physics, 118(22), 10174-10182.

Ohta, K., Hirose, K., Onoda, S., and Shimizu, K. (2007) The effect of iron spin transition on electrical conductivity of (Mg,Fe)O magnesiowustite. Proceedings of the Japan Academy Series B-Physical and Biological Sciences, 83(3), 97-100.

Perdew, J.P., Burke, K., and Ernzerhof, M. (1996) Generalized gradient approximation made simple. Physical Review Letters, 77(18), 3865-3868.

Piet, H., Badro, J., Nabiei, F., Dennenwaldt, T., Shim, S.H., Cantoni, M., Hebert, C., and Gillet, P. (2016) Spin and valence dependence of iron partitioning in Earth's deep mantle. Proceedings of the National Academy of Sciences of the United States of America, 113(40), 11127-11130.

Runcorn, S.K. (1992) Polar Path in Geomagnetic Reversals. Nature, 356(6371), 654-656.

Schifferle, L., and Lobanov, S.S. (2022) Evolution of Chemical Bonding and Spin-Pairing Energy in Ferropericlase across Its Spin Transition. Acs Earth and Space Chemistry, 6(3), 788-799.

DOI: https://doi.org/10.2138/am-2023-9100. http://www.minsocam.org/

Schifferle, L., Speziale, S., and Lobanov, S.S. (2022) High-pressure evolution of the refractive index of MgO up to 140 GPa. Journal of Applied Physics, 132(12), 125903.

Shannon, R.D., and Fischer, R.X. (2016) Empirical electronic polarizabilities of ions for the prediction and interpretation of refractive indices: Oxides and oxysalts. American Mineralogist, 101(9-10), 2288-2300.

Sherman, D.M., and Waite, T.D. (1985) Electronic spectra of Fe^{3+} oxides and oxide hydroxides in the near IR to near UV. American Mineralogist, 70(11-12), 1262-1269.

Song, Y.L., He, K.H., Sun, J., Ma, C.J., Wan, M., Wang, Q.B., and Chen, Q.L. (2019) Effects of iron spin transition on the electronic structure, thermal expansivity and lattice thermal conductivity of ferropericlase: a first principles study. Scientific Reports, 9.

Stephens, R.E., and Malitson, I.H. (1952) Index of refraction of magnesium oxide. Journal of Research of the National Bureau of Standards, 49(4), 249-252.

Sun, Y., Zhuang, J., and Wentzcovitch, R.M. (2022) Thermodynamics of spin crossover in ferropericlase: an improved LDA + Usc calculation. Electronic Structure, 4(1), 014008.

Tauc, J. (1968) Optical properties and electronic structure of amorphous Ge and Si. Materials Research Bulletin, 3(1), 37-46.

van Straaten, J., and Silvera, I.F. (1988) Equation of state of solid molecular H_2 and D_2 at 5 K. Physical Review B, 37(4), 1989-2000.

Velimsky, J., and Knopp, O. (2021) Lateral variations of electrical conductivity in the lower mantle constrained by Swarm and CryoSat-2 missions. Earth Planets and Space, 73(1).

Walt, S.v.d., Colbert, S.C., and Varoquaux, G. (2011) The NumPy Array: A Structure for Efficient Numerical Computation. Computing in Science & Engineering, 13(2), 22-30.

Wemple, S.H., and DiDomenico, M. (1971) Behavior of the Electronic Dielectric Constant in Covalent and Ionic Materials. Physical Review B, 3(4), 1338-1351.

Womes, M., and Jumas, J.C. (2013) Effect of Fe(II) spin crossover on charge distribution in and lattice properties of thiospinels. Journal of Physics and Chemistry of Solids, 74(3), 457-465.

Wood, B.J., and Nell, J. (1991) High-Temperature Electrical Conductivity of the Lower Mantle Phase (Mg,Fe)O. Nature, 351(6324), 309-311.

Zha, C.S., Hemley, R.J., Gramsch, S.A., Mao, H.K., and Bassett, W.A. (2007) Optical study of H_2O ice to 120 GPa: Dielectric function, molecular polarizability, and equation of state. Journal of Chemical Physics, 126(7), 074506.